Title

Longitudinal tau accumulation and atrophy in aging and alzheimer disease

Permalink

https://escholarship.org/uc/item/91z4z1qs

Authors

Harrison, Theresa M
La Joie, Renaud
Maass, Anne
et al.

Longitudinal Tau Accumulation and Atrophy in Aging and Alzheimer Disease

Theresa M. Harrison, PhD[1], **Renaud La Joie, PhD**[2], **Anne Maass, PhD**[1,3], **Suzanne L. Baker, PhD**[4], **Kaitlin Swinnerton, BS**[1], **Laura Fenton, BA**[1], **Taylor J. Mellinger, BS**[2], **Lauren Edwards, BS**[2], **Julie Pham, BA**[2], **Bruce L. Miller, MD**[2], **Gil D. Rabinovici, MD**[2], and **William J. Jagust, MD**[1,4]

[1]Helen Wills Neuroscience Institute, University of California, Berkeley, Berkeley, CA

[2]Memory and Aging Center, University of California, San Francisco, San Francisco, CA

[3]German Center for Neurodegenerative Diseases, Magdeburg, Germany

[4]Lawrence Berkeley National Laboratory, Berkeley, CA

Abstract

Objective—To determine the rate of tau accumulation in healthy older adults (OA) and patients with Alzheimer disease (AD), as well as the relationship of tau accumulation to cortical atrophy.

Methods—Two longitudinal flortaucipir (FTP) positron emission tomography (PET) and magnetic resonance imaging (MRI) scans were acquired from 42 OA (21 Pittsburg compound B [PiB]$^+$, age = 77.6 ± 4.6 years, 25 female [F]/17 male [M]) and 19 PiB$^+$ patients with AD (age = 63.1 ± 10.3 years, 12 F/7 M) over 1 to 3 years of follow-up. FTP change, structural MRI measures of atrophy, and cross-modal correlations were examined on a voxelwise level. Regional annual percentage change in FTP was also calculated.

Results—Voxelwise FTP change in AD showed the greatest increases in lateral and medial frontal lobes. Atrophy over the same interval was more widespread and included posteromedial cortical areas, where tau accumulation rates were lower. In OA, FTP binding increased in bilateral temporal lobe and retrosplenial cortex, accompanied by atrophy in the same regions. There were no associations between voxelwise change in FTP and sex, PiB, or *APOE*. Regional FTP significantly increased at follow-up in OA and patients with AD. Mixed effects models showed greater FTP increases in AD compared to OA, and no differences within OA based on PiB status.

Interpretation—Our findings indicate that tau accumulates even in amyloid-negative healthy OA and this process can be measured with in vivo tau-PET. In OA, tau accumulation and atrophy share a similar topography. In AD, tau increases more rapidly and accumulation occurs in frontal regions that are not yet undergoing significant atrophy.

Accumulation of hyperphosphorylated tau in intracellular neurofibrillary tangles (NFTs) is a hallmark of Alzheimer disease (AD)[1] and is common in healthy aging.[2] The topology of tau, however, differs in patients with AD compared to cognitively healthy older adults (OA). Based on cross-sectional autopsy studies in both aging and disease, cortical tau accumulation appears to begin in the transentorhinal region of the medial temporal lobe (MTL) and spreads to neighboring regions in ventral and lateral temporal lobe, as well as retrosplenial cortex and posterior cingulate.[3] In AD, tau accumulation becomes more widespread, affecting large areas of neocortex. The neurobiological distinction between early tau accumulation in normal aging compared to AD, which is marked by subsequent severe tauopathy, remains unclear.

Flortaucipir (FTP; [^{18}F]-AV-1451) is a tau positron emission tomography (PET) tracer that binds to paired helical filament tau within NFTs.[4] Since the recent advent of tau-PET imaging, several cross-sectional studies have shown that FTP retention in vivo reveals patterns consistent with the known neuropathological topology of NFTs.[5–9] Furthermore, FTP signal has been shown to relate to cognition in normal controls and patients with AD.[5–10] Very few studies, however, have examined longitudinal FTP imaging.[11,12] These longitudinal studies employed markedly different methods and reported conflicting results in regard to rate of FTP accumulation, highlighting the need for further exploration of the optimal methods for analyzing longitudinal FTP data. Importantly, optimal methods for quantification of cross-sectional and longitudinal PET data are not necessarily in agreement, especially in reference region selection.[13–16]

Postmortem studies have shown that the accumulation of NFTs is related to cognitive deficits[17,18] and to neurodegeneration, although data suggest other independent mechanisms also drive synaptic dysfunction and neuronal loss.[19,20] Imaging studies reveal a strong relationship between FTP binding and atrophy in cross-sectional cohorts, which indicates that these pathologies likely interact over time.[10,21] Normal aging is accompanied by a stereotyped pattern of cortical thinning but, similar to the accumulation and spread of tau, there is an acceleration of this process manifesting as frank neurodegeneration in AD. It is unclear whether longitudinal changes in FTP are related to longitudinal cortical shrinkage and how this relationship may compare in AD and typical healthy aging.

To address these gaps in our understanding of longitudinal FTP and its correlates, we aimed to develop an analytic approach optimized to sensitively measure FTP change, even in OA, and relate that change to neurodegeneration, also measured in vivo. To that end, the present study had 2 main goals: first, to identify the magnitude and pattern of FTP change in OA and patients with AD and second, to compare the spatial correspondence between FTP accumulation and cortical atrophy during the same interval. We predicted that FTP accumulation would be more pronounced in AD compared to OA, and that, within OA, β-amyloid (Aβ) burden would be related to FTP rate of change. We further predicted that regional distributions of FTP accumulation and atrophy would differ between patients with AD and OA.

Subjects and Methods

Participants

The present study included 2 cohorts: 42 cognitively healthy OA enrolled in the Berkeley Aging Cohort Study (BACS) and 19 patients with probable AD recruited from the University of California, San Francisco (UCSF) Alzheimer's Disease Research Center. OA participants are part of an ongoing longitudinal study of normal cognitive aging. Each participant in the present study had no imaging contraindications and had undergone baseline tau-PET imaging with FTP, Aβ-PET imaging with Pittsburg compound B (PiB), and 1.5T structural magnetic resonance imaging (sMRI), as well as follow-up FTP and sMRI scans. Each OA participant completed a neuropsychological testing session at baseline and follow-up. Most of the OA participants also had at least one annual neuropsychological testing session preceding the baseline imaging visit (n = 37). Additional inclusion criteria included a baseline Mini-Mental State Examination (MMSE) score 25, no neurological, psychiatric, or major medical illness, no medications affecting cognition, and that all participants were community-dwelling. The institutional review board (IRB) at Lawrence Berkeley National Laboratory (LBNL) and the University of California, Berkeley approved the BACS project, and written, informed consent was obtained from all BACS participants.

UCSF participants underwent a clinical evaluation including neurological history, physical and neurological examinations, structured caregiver interviews, 3T sMRI, and neuropsychological testing. Clinical diagnosis was determined by consensus of a multidisciplinary team of experts. All UCSF participants had a positive PiB scan (established by both visual read and quantitatively) and met criteria for probable AD or mild cognitive impairment due to AD.[22,23] In addition, 5 patients met criteria for posterior cortical atrophy and 1 for the logopenic variant of primary progressive aphasia.[24,25] UCSF participants received baseline FTP and PiB scans as well as follow-up FTP and MRI scans. Informed consent was obtained from all patients or their surrogates, and the IRB at UCSF and at LBNL approved the study.

Cognitive Assessment

Neuropsychological assessments for BACS and patients with AD from UCSF have been previously described.[10,26] Briefly, BACS subjects undergo testing to measure performance on global cognitive (eg, MMSE) and specific cognitive tasks including those related to verbal and visual memory, working memory, processing speed, executive function, language, and attention. UCSF patients with AD are assessed for episodic and semantic memory, language, and executive and visuospatial functioning as well as global functioning with the MMSE and the Clinical Dementia Rating (CDR) scale.

APOE *Genotyping*

Determination of *APOE* alleles was performed as described previously using a TaqMan Allelic Discrimination Assay using a Real-Time PCR system (Applied Biosystems, Foster City, CA).[27] *APOE* genotyping was completed for 41 OA and all 19 patients with AD.

Image Acquisition

Detailed descriptions of FTP and PiB PET acquisition are available in previous publications.[5,7] All PET scans for both cohorts were acquired at LBNL on a Siemens (Erlangen, Germany) Biograph 6 Truepoint PET/computed tomography (CT) scanner in 3-dimensional acquisition mode. Prior to each PET scan, a low-dose CT scan was collected for attenuation correction. FTP was synthesized at the LBNL Biomedical Isotope Facility (BIF) using a TracerLab FXN-Pro (GE Medical Systems, Milwaukee, WI) synthesis module with a modified protocol based on an Avid Radiopharmaceuticals (Philadelphia, PA) protocol supplied to the facility. Participants were injected with 10 mCi of tracer and scanned in listmode 80 to 100 minutes postinjection (4×5-minute frames). [^{11}C] PiB was also synthesized at the LBNL BIF according to a previously published protocol.[28] Beginning at the start of an injection of 15 mCi of PiB into an antecubital vein, 90 minutes of dynamic emission data were acquired and subsequently binned into 35 frames (4×15, 8×30, 9×60, 2×180, 10×300, and 2×600 seconds). FTP and PiB images were reconstructed using an ordered subset expectation maximization algorithm with weighted attenuation and smoothed with a 4 mm Gaussian kernel with scatter correction (image resolution = $6.5 \times 6.5 \times 7.25$ mm^3).

High-resolution T1-weighted magnetization-prepared rapid gradient echo (MPRAGE) sMRI scans were acquired for each BACS participant with the following parameters: sagittal slice orientation, repetition time (TR) = 2,110 milliseconds, echo time (TE) = 3.58 milliseconds, flip angle = 15°, voxel size = 1 mm isotropic. These data were collected on a 1.5T Siemens Magnetom Avanto scanner at LBNL. High-resolution T1-weighted MPRAGE data were acquired for UCSF participants on either a 3T Siemens Tim Trio or 3T Siemens Prisma Fit scanner with the following parameters: sagittal slice orientation, voxel size = 1 mm isotropic, matrix = 240×256, TR = 2,300 milliseconds, TE = 2.9 milliseconds (2.98 milliseconds on the Trio), inversion time = 900 milliseconds, flip angle = 9°. Six UCSF participants were scanned on the Trio at baseline and the Prisma at follow-up, which did not systematically affect atrophy measurements.

Image Processing

FTP standardized uptake value ratio (SUVR) images were created based on mean tracer uptake 80 to 100 minutes postinjection.[29] Based on pilot analyses, a longitudinal preprocessing pipeline was established that allowed for voxelwise analyses of change over time in both FTP and sMRI data, and used a single unbiased reference region for both baseline and follow-up FTP data. Specifically, sMRI scans from baseline and follow-up visits were used to create a midpoint, average sMRI image using SPM12[30] and SUVR images from baseline and follow-up were registered to this midpoint subject space. Midpoint sMRI scans were processed with FreeSurfer[31] for region of interest (ROI) analyses and segmented with SPM12. The white matter (WM) segment from each participant's midpoint sMRI was thresholded at 0.95 and then eroded by 1 voxel. This participant-specific WM ROI in midpoint sMRI subject space was used to normalize the baseline and follow-up FTP data. We chose to use a white matter reference region because this approach resulted in more stable estimates of change over time, especially in OA. FTP change images were created by subtracting the FTP value at baseline from the value at follow-up for each voxel in midpoint

sMRI subject space. DARTEL[32] tools were then used to warp the following images to Montreal Neurological Institute (MNI) space: sMRIs, gray matter (GM)-masked Jacobian determinants, and FTP change images. Once in standard space, FTP change images were multiplied by an inclusive, group-specific intracranial mask and then smoothed with a $6mm^3$ Gaussian kernel. GM-masked Jacobian images were smoothed with an $8mm^3$ Gaussian kernel and were used for longitudinal voxel-based morphometry (VBM) analyses.[30] Voxelwise annual percentage change (APC) maps were also created by calculating APC at every voxel in midpoint sMRI subject space. Individual participant APC maps were then warped to MNI space with DARTEL, and group mean APC images were used to quantify effect size of change in FTP.

ROI analyses of FTP data were performed using Geometric Transfer Matrix partial volume correction (PVC) on FreeSurfer ROIs derived from the midpoint sMRI.[33,34] PVC FTP SUVRs from ROIs defined based on concurrent sMRI (without creating a midpoint sMRI image) were correlated with SUVRs derived from our longitudinal approach at $r > 0.94$. Results of ROI analyses did not change based on ROI definition method. Therefore, we used a single processing approach that resulted in unbiased estimates of the reference region and allowed us to complete both voxelwise and ROI analyses. APC was calculated for mean PVC SUVR values in 6 a priori ROIs: entorhinal cortex (ERC), inferior temporal lobe (IT), retrosplenial cortex (RSC), posterior cingulate cortex (PCC), a temporal lobe meta region[35] (Meta ROI), and a region corresponding to Braak stage III/IV.[9,34]

Distribution volume ratios (DVRs) for PiB images were generated with Logan graphical analysis on PiB frames corresponding to 35 to 90 minutes postinjection using a cerebellar GM reference region.[36,37] Participants were determined to be Aβ-positive (PiB⁺) based on a mean global cortical DVR > 1.065 at the baseline visit (patients with AD were also positive based on visual read).[38]

Statistical Analysis

In each cohort, using voxelwise data, general linear models (GLMs) covarying for age and interval between scans were used to determine regions where tau had significantly increased at follow-up (ie, 1-sample *t* tests with covariates). Mean group (OA or AD) APC was calculated for each voxel in regions where tau was significantly increasing at the group level based on the 1-sample *t* test (voxel $p < 0.001$, cluster familywise error [FWE] $p < 0.05$ in OA; voxel $p < 0.001$, uncorrected in AD). Different statistical thresholds for OA and AD were used to reduce bias resulting from differing statistical power in our cohorts of 42 and 18 participants, respectively. Statistical thresholds were kept consistent across modalities within group so FTP–atrophy associations could be measured within group. We also created masks based on the regions that were significant in each group, resulting in 2 different masks, 1 for OA and 1 for AD. Next, we calculated mean voxelwise APC in OA and AD masks for each participant. A 1-way repeated measures analysis of variance (ANOVA) was used to determine the effect of group on mean APC (repeated measures are participant mean SUVR APC in OA and AD masks). In OA, a 2-sample *t* test was used to determine whether there were differences in FTP accumulation based on PiB status. In addition, baseline PiB DVR was treated as a continuous variable of interest in a GLM predicting voxelwise FTP

change. To reveal regions of significant atrophy, voxelwise Jacobian determinants accounting for scan interval were used to run GLMs controlling for age.

One sample t tests were used to determine whether group mean APC in ROIs was significantly greater than zero. Pearson correlations were used to test for significant associations between baseline PiB DVR and FTP APC in each ROI. Linear mixed effects (LME) models were used to predict repeated measures of FTP in each ROI with fixed effects of age, sex, PiB status, and years from baseline as well as a random effect for participant intercept. An LME model that included only OA participants was fitted to test for an interaction effect between PiB status and time on regional FTP change.

Results

Participants

Characteristics of the OA and AD cohorts are summarized in Table 1. OA were significantly older than AD subjects ($p < 0.001$), and the groups did not differ on sex composition or education. In the OA cohort, 34% (n = 14) carried the APOEε4 allele; 53% (n = 10) of patients with AD were APOEε4 carriers. By design, all patients with AD were PiB$^+$, whereas 50% (n = 21) of OA were PiB$^+$. Importantly, in the OA cohort PiB$^+$ subjects were slightly younger than the PiB$^-$ subjects (PiB$^+$: 76.2 ± 3.9 years, PiB$^-$: 79.0 ± 5.0 years; $p =$ 0.048). This is likely due our FTP-PET recruitment strategy, which initially oversampled older and/or PiB$^+$ participants in the OA group.

Within baseline and follow-up visits, sMRI scans were acquired on average 1.1 ± 3.0 months before FTP scans in the OA cohort and 1.1 ± 1.8 months before FTP in the patients with AD. PiB scans were acquired 0.9 ± 2.7 months before the FTP scans in the OA cohort. In the AD cohort, all PiB scans were acquired on the same day as FTP scans except for 1 patient whose PiB scan was 4.9 months before their FTP scan. One patient with AD was not included in FTP voxelwise analyses or longitudinal VBM because midpoint sMRI registration failed. Another patient with AD was excluded from ROI analyses due to unresolvable parcellation errors in FreeSurfer.

Voxelwise Analyses: Longitudinal FTP

At baseline, FTP signal in OA was highest in MTL, with slightly elevated mean signal in ventral and lateral temporal lobes as well as posterior medial and orbitofrontal regions (Fig 1). In AD, FTP mean and peak signal was higher compared to OA and the predominant topology included temporal, lateral parietal, and posterior medial regions. The results of the longitudinal voxelwise FTP change analyses in OA are shown in Figure 2A. FTP significantly increased in bilateral temporal lobes and retrosplenial cortex, as well as small clusters in left frontal lobe (voxel $p < 0.001$, cluster FWE $p < 0.05$). The pattern in the temporal lobe was slightly asymmetric, with greater involvement of the left inferior temporal lobe, fusiform gyrus, and parahippocampal gyrus than the homologous regions on the right. In AD, the pattern of increases in FTP predominantly involved lateral and medial frontal lobe, left greater than right (voxel $p < 0.001$, uncorrected; see Fig 2). At the more conservative statistical threshold used for OA, only the left hemisphere medial and lateral

frontal regions show significant FTP increases in AD. There were no significant decreases in FTP binding in either cohort. OA and AD FTP significant increase masks overlaid on voxelwise group mean APC maps showed significant FTP increases of 2 to 3% per year in OA and 3 to 6% per year in AD. OA and AD FTP increase masks were also used to calculate mean APC for each participant in each mask. A 1-way repeated measures ANOVA revealed significant effects of mask, group, and the mask × group interaction (all $p < 0.001$; Supplementary Table). Post hoc tests revealed that FTP increases in AD were not significantly greater than in OA in the OA mask (Tukey $p = 0.99$). There was no significant difference between AD APC in the OA mask and OA APC in the AD mask (Tukey $p = 0.59$), but all other group by mask post hoc tests showed significant differences (all Tukey $p < 0.05$).

Voxelwise Analyses: Longitudinal VBM

To relate longitudinal FTP change to structural change over the same follow-up interval, we completed longitudinal VBM analyses. In OA, a posterior predominant pattern of cortical volume loss was observed (voxel $p < 0.001$, cluster FWE $p < 0.05$; Fig 3A). Large areas of temporal, parietal, and medial occipital lobe significantly decreased in volume, whereas the frontal lobe was relatively spared. In AD, the pattern of atrophy was similar but did not include medial occipital regions (voxel $p < 0.001$, uncorrected; see Fig 3D).

Voxelwise Analyses: Cross-Modal Associations

The spatial overlap of regions with significant FTP increase and regions with significant atrophy are shown for OA in Figure 3B and for AD in Figure 3E. In OA, there was overlap between regions of FTP increase and GM loss. In AD, however, the overlap was minimal, with FTP increases occurring in frontal regions, and atrophy predominating in posterior regions. We plotted GM voxelwise group statistical maps for FTP increase and atrophy and fit linear models to quantify the strength of the correlations (see Fig 3C, F). In OA, FTP change explained 21.2% of the variance in atrophy, whereas this relationship was not meaningful in AD, explaining only 2.7% of the variance.

ROI Analyses: APC

Patients with AD had higher FTP SUVR than OA at baseline across all examined ROIs ($p < 0.001$; Table 2). OA showed significant regional increases in FTP at follow-up across all a priori ROIs ($p < 0.001$), and patients with AD showed significant increases in IT, RSC, the Meta ROI, and the Braak III/IV ROI ($p \quad 0.008$). Mean APC in FTP was higher in AD compared to OA in the Meta and Braak III/IV ROIs ($p < 0.05$), larger regions where variance was smaller relative to the mean. Results were similar if annual difference in SUVR (SUVR per year) was used as the change metric. Longitudinal regional FTP data are plotted in Figure 4. Spaghetti plots show individual trajectories of change over time in raw SUVR, whereas boxplots highlight the interindividual variance in APC in each ROI. There were no significant differences in APC between PiB$^+$ and PiB$^-$ OA in any ROI ($p > 0.30$). Furthermore, in OA there were no significant associations between PiB DVR at baseline and APC in any a priori ROI ($p > 0.50$).

Results from voxelwise analyses revealed regions of frontal lobe with baseline FTP signal and significant FTP change in OA. As an exploratory analysis, we also examined 2 frontal ROIs: orbitofrontal cortex (FOrb; includes frontal pole ROI) and inferior frontal gyrus (IFG; comprised of pars orbitalis, pars triangularis, and pars opercularis). Patients with AD had higher FTP SUVR at baseline in FOrb and IFG ($p < 0.001$; see Table 2). FTP signal significantly increased at follow-up for both frontal ROIs in OA and AD, and AD patients had greater APC compared to OA ($p < 0.05$).

ROI Analyses: LME Models

LME models controlling for age and sex produced results consistent with regional APC analyses. Across ROIs, there was a main effect of group such that patients with AD had greater FTP than OA across all timepoints ($p < 0.001$; Fig 5). There was also a significant time by group effect such that AD patients' FTP increased more than that of OA in IT, the Meta ROI, and Braak III/IV ROI ($p < 0.01$). The time by group effect comparing AD to OA was not significant in the ERC, RSC, or PCC ROIs ($p > 0.2$). There were no differences in rate of change between PiB$^+$ and PiB$^-$ OA participants in any ROI in the full model or in models fitted with just OA participants. Full model parameter estimates for models predicting ERC, Meta ROI, and Braak III/IV FTP are provided in Table 3.

Discussion

We addressed the first main goal of our study by employing voxelwise and ROI-based approaches to measure the magnitude of FTP change over time in OA (~2–3% per year) and patients with AD (~3–6% per year). The spatial topology of FTP accumulation in OA was predominantly temporal and medial parietal, and differed from the pattern in AD, which was predominantly frontal. Although we did not find that PiB$^+$ OA accumulated FTP faster than PiB$^-$ OA, we showed significant FTP accumulation over an average 1.9-year follow-up in the whole OA group.

To address our second goal, we used voxelwise, whole brain data to reveal a pattern of FTP accumulation that was consistent with known topology and spread of tau pathology in aging. Strikingly, the pattern of FTP accumulation resembled the pattern of concurrent atrophy in the OA participants. Regions where FTP increased in OA were also similar to the areas where FTP binding was detected at baseline. In contrast, in AD, FTP increased in frontal regions outside of the areas of major FTP binding at baseline. This indicates that areas of high baseline FTP binding in symptomatic patients with AD are no longer rapidly accumulating pathology across individuals, but rather "downstream" regions associated with greater disease severity are the areas with the most marked tau accumulation. Consistent with this, the pattern of atrophy in AD also more closely resembled baseline FTP binding and did not spatially correspond to the pattern of FTP increases.

The differing spatial relationships between FTP increases and atrophy in OA and AD may reflect a temporal lag between tau pathology and subsequent neurodegeneration that widens in the clinical phase of the disease as tau accumulation and spread accelerate. In contrast, the initial phase of tau spread in cognitively intact OA is an indolent process accompanied by atrophy in overlapping areas. The distinction between AD and OA may reflect acceleration

of tau deposition in AD, or greater vulnerability to tau in temporoparietal cortex than prefrontal regions. Both possibilities are consistent with the finding that FTP accumulation in AD did not differ from OA in regions where OA FTP was significantly increasing (see Fig 2A). It is also possible that the rate of tau accumulation slows over time, similar to amyloid accumulation.[39]Regardless of interpretation, it is important to note that voxelwise analyses were completed without PVC, which may affect our ability to detect FTP changes in atrophic brain regions. Previous work has shown that cross-sectional FTP is associated with cross-sectional atrophy patterns in AD,[10,21] but our study extends these findings by revealing that FTP longitudinal accumulation occurs in regions that are relatively less affected by atrophy.

Regional PVC analyses revealed significant FTP increases in both OA and AD across multiple ROIs. Patients with AD had significantly greater accumulation in the 2 larger ROIs we examined, the temporal Meta ROI and Braak III/IV regions, but there was no significant difference in mean FTP change in ERC between OA and AD, consistent with other reports. [11] These ROI findings could reflect greater ability to detect change due to higher signal to noise in the larger regions, or a slowing of tau deposition in the ERC, which is the first cortical region affected. In contrast to previous data showing a lack of FTP increase in Aβ-negative normal adults, we found that FTP increased across ROIs in our OA cohort.[11,12] We did not observe a difference in FTP change between PiB⁺ and PiB⁻ groups. Across the OA group, our estimates of APC were higher than previous work, which measured 0.5% APC in PiB⁺ normal controls.[11] Human and animal data suggest that Aβ pathology is important in facilitating the spread of tau.[40–42] Thus, we hypothesized that PiB⁺ OA would have higher rates of FTP accumulation than PiB⁻ OA. That we did not observe this is likely related to our limited sample size, and also to the age of our OA participants. PiB⁻ OA participants in our study were slightly older than the PiB⁺ OA participants, and the mean age for the entire group was 77.6 years. In a true random sample, we would expect PiB⁺ OA to be older on average than PiB⁻ individuals. In a recent large study of longitudinal FTP that reported differences in FTP change based on PiB status, the PiB⁺ group had a median age of 80 years, whereas in the PiB⁻ group median age was 66 years.[11] It is also possible that the difference in FTP accumulation rate between PiB⁺ and PiB⁻ individuals is too subtle to detect over the ~2-year follow-up in our sample.

Previous studies examining longitudinal FTP have used different reference regions, and it remains unclear which approach is optimal.[11,12] Work in our laboratory has indicated that FTP signal in WM and GM are still correlated even after PVC. Our choice of a WM reference region, derived from midpoint sMRI subject space, corrects for this shared signal. WM reference regions have previously been shown to be superior for longitudinal analyses of Aβ PET tracers,[13–15] and WM reference regions perform better on 4-week test–retest FTP data (variability from 1.7 to 2.8%) than GM reference regions.[12] Another possible advantage of WM as a reference is the relatively large size of the region, as nonspecific signal in larger regions is likely to be more stable over time. It has also been argued that reference regions that share the same axial location as ROIs correct for differences in perfusion, to which SUVR values are extremely sensitive.[43] A risk of our approach is that true FTP signal from cortex may bleed into the reference region despite our thresholding and erosion steps. This could explain the differences between our findings and those of

Southekal and colleagues, who also used a WM reference region optimized to minimize signal contamination.[12] Our results, however, indicate our approach is a robust way to measure the spatial topography of FTP change.

Evidence from model systems has emerged supporting a theory that hyperphosphorylated tau spreads trans-synaptically through circuits and propagates in a prion-like manner.[44,45] Given that tau accumulation appears to begin in the transentorhinal cortex, it is hypothesized that tau first spreads through the memory circuitry of the temporal lobe. This is supported by Braak staging which, as a neuropathological staging scheme, is unavoidably crosssectional. Our results with in vivo longitudinal FTP-PET also support this model of tau propagation with baseline levels of FTP highest in MTL and FTP increasing in MTL-connected posteromedial regions such as retrosplenial cortex, and anterior regions such as inferior temporal gyrus and inferior frontal cortex.[46] The MTL is connected to these regions via the cingulum bundle and the uncinate fasciculus, two key structural pathways underlying normal memory function through which tau may spread. The wider involvement of these memory circuits is in line with findings from Jack and colleagues, who showed that early accumulation of tau pathology is not limited to ERC, despite Braak staging indicating otherwise.[11] Importantly, our data also suggest that tau spread occurs outside the MTL in Aβ-negative individuals, which indicates that either peri-MTL tau accumulation is not entirely dependent on Aβ or that Aβ species undetectable by PET are involved in the earliest propagation of tau across networks.

Our study has several limitations. First, our small sample size may have limited our statistical power in general and especially to detect differences in rate of accumulation between PiB⁺ and PiB⁻ OA. Second, our cohort of patients with AD included individuals with less common phenotypes, such as posterior cortical atrophy and individuals with early onset AD. Thus, our UCSF AD cohort is significantly younger than our community-dwelling OA, and our findings may be less generalizable to the more common late onset AD (LOAD). It is likely that the topography and rate of tau accumulation differs in LOAD compared to our less typical, early onset cases. Therefore, further studies are needed to assess the relationship between tau accumulation and atrophy in LOAD. One benefit of the younger clinical cohort is that we can reasonably be more assured that the clinical syndrome is caused by AD pathology and not markedly exacerbated by age-related comorbidities, like advanced neurovascular disease or other proteinopathies. Another limitation of the present study is the known off-target binding of FTP in the basal ganglia, especially the putamen and pallidum, which may be related to age-related iron deposition.[47] FTP also often binds to choroid plexus and the meninges, and has been shown to bind to incidental findings on MRI (eg, meningiomas, cavernous malformations).[48] These off-target sources of signal are unlikely to have driven our results, because we applied PVC for regional analyses, and the voxelwise FTP increases were seen in brain areas remote from off-target binding sites.

Because FTP-PET has been available for a relatively short time, large longitudinal datasets are not available yet. The optimal methods for processing these data and their potential utility for both basic neuroscience and translational applications remain unclear. Here we show that using an explicitly longitudinal approach to preprocessing allowed us to identify voxelwise FTP change patterns in OA and a cohort of patients with AD. Our findings

demonstrate the temporospatial relationship of FTP increase and atrophy is different in typical aging and disease. Future work will focus on causal relationships between markers of tau pathology and subsequent atrophy as well as cognitive trajectory.

Supplementary Material

Refer to Web version on PubMed Central for supplementary material.

Acknowledgment

References

1. Grundke-Iqbal I, Iqbal K, Tung YC, et al. Abnormal phosphorylation of the microtubule-associated protein tau (tau) in Alzheimer cytoskeletal pathology. Proc Natl Acad Sci U S A 1986;83:4913–4917. [PubMed: 3088567]

2. Knopman DS, Parisi JE, Salviati A, et al. Neuropathology of cognitively normal elderly. J Neuropathol Exp Neurol 2003;62:1087–1095. [PubMed: 14656067]

3. Braak H, Braak E. Neuropathological stageing of Alzheimer-related changes. Acta Neuropathol 1991;82:239–259. [PubMed: 1759558]

4. Marquié M, Normandin MD, Vanderburg CR, et al. Validating novel tau positron emission tomography tracer [F-18]-AV-1451 (T807) on postmortem brain tissue Ann Neurol 2015;78:787–800. [PubMed: 26344059]

5. Ossenkoppele R, Schonhaut DR, Schöll M, et al. Tau PET patterns mirror clinical and neuroanatomical variability in Alzheimer's disease. Brain 2016;139:1551–1567. [PubMed: 26962052]

6. Johnson KA, Schultz A, Betensky RA, et al. Tau PET imaging in aging and early Alzheimer's disease. Ann Neurol 2015;79:110–119. [PubMed: 26505746]

7. Schöll M, Lockhart SN, Schonhaut DR, et al. PET imaging of tau deposition in the aging human brain. Neuron 2016;89:971–982. [PubMed: 26938442]

8. Schwarz AJ, Yu P, Miller BB, et al. Regional profiles of the candidate tau PET ligand ^{18}F-AV-1451 recapitulate key features of Braak histopathological stages. Brain 2016;139:1539–1550. [PubMed: 26936940]

9. Maass A, Lockhart SN, Harrison TM, et al. Entorhinal tau pathology, episodic memory decline, and neurodegeneration in aging. J Neurosci 2018;38:530–543. [PubMed: 29192126]

10. Bejanin A, Schonhaut DR, La Joie R, et al. Tau pathology and neurodegeneration contribute to cognitive impairment in Alzheimer's disease. Brain 2017;140:3286–3300. [PubMed: 29053874]

11. Jack CR, Wiste HJ, Schwarz CG, et al. Longitudinal tau PET in ageing and Alzheimer's disease. Brain 2018;141:1517–1528. [PubMed: 29538647]

12. Southekal S, Devous MD, Kennedy I, et al. Flortaucipir F 18 quantitation using parametric estimation of reference signal intensity. J Nucl Med 2018;59:944–951. [PubMed: 29191858]

13. Fleisher AS, Joshi AD, Sundell KL, et al. Use of white matter reference regions for detection of change in florbetapir positron emission tomography from completed phase 3 solanezumab trials. Alzheimers Dement 2017;13:1117–1124. [PubMed: 28365320]

14. Chen K, Roontiva A, Thiyyagura P, et al. Improved power for characterizing longitudinal amyloid-PET changes and evaluating amyloidmodifying treatments with a cerebral white matter reference region. J Nucl Med 2015;56:560–566. [PubMed: 25745091]

15. Schwarz CG, Senjem ML, Gunter JL, et al. Optimizing PiB-PET SUVRchange-over-time measurement by a large-scale analysis of longitudinal reliability, plausibility, separability, and correlation with MMSE. Neuroimage 2017;144:113–127. [PubMed: 27577718]

16. Rasmussen JM, Lakatos A, van Erp TG, et al. Empirical derivation of the reference region for computing diagnostic sensitive ^{18}fluorodeoxyglucose ratios in Alzheimer's disease based on the ADNI sample. Biochim Biophys Acta 2012;1822:457–466. [PubMed: 21958592]

17. Giannakopoulos P, Herrmann FR, Bussière T, et al. Tangle and neuron numbers, but not amyloid load, predict cognitive status in Alzheimer's disease. Neurology 2003;60:1495–1500. [PubMed: 12743238]

18. von Gunten A, Kövari E, Bussière T, et al. Cognitive impact of neuronal pathology in the entorhinal cortex and CA1 field in Alzheimer's disease. Neurobiol Aging 2006;27:270–277. [PubMed: 16399212]

19. Spires-Jones TL, Hyman BT. The intersection of amyloid beta and tau at synapses in Alzheimer's disease. Neuron 2014;82:756–771. [PubMed: 24853936]

20. Gómez-Isla T, Hollister R, West H, et al. Neuronal loss correlates with but exceeds neurofibrillary tangles in Alzheimer's disease. Ann Neurol 1997;41:17–24. [PubMed: 9005861]

21. Xia C, Makaretz SJ, Caso C, et al. Association of in vivo [18F]AV-1451 tau PET imaging results with cortical atrophy and symptoms in typical and atypical Alzheimer disease. JAMA Neurol 2017;74:427–436. [PubMed: 28241163]

22. McKhann GM, Knopman DS, Chertkow H, et al. The diagnosis of dementia due to Alzheimer's disease: recommendations from the National Institute on Aging-Alzheimer's Association workgroups on diagnostic guidelines for Alzheimer's disease. Alzheimers Dement 2011;7:263–269. [PubMed: 21514250]

23. Albert MS, DeKosky ST, Dickson D, et al. The diagnosis of mild cognitive impairment due to Alzheimer's disease: recommendations from the National Institute on Aging-Alzheimer's Association workgroups on diagnostic guidelines for Alzheimer's disease. Alzheimers Dement 2011;7:270–279. [PubMed: 21514249]

24. Crutch SJ, Schott JM, Rabinovici GD, et al. Consensus classification of posterior cortical atrophy. Alzheimers Dement 2017;13:870–884. [PubMed: 28259709]

25. Gorno-Tempini ML, Hillis AE, Weintraub S, et al. Classification of primary progressive aphasia and its variants. Neurology 2011;76: 1006–1014. [PubMed: 21325651]

26. Harrison TM, Maass A, Baker SL, Jagust WJ. Brain morphology, cognition, and β-amyloid in older adults with superior memory performance. Neurobiol Aging 2018;67:162–170. [PubMed: 29665578]

27. Coppola G, Chinnathambi S, Lee JJ, et al. Evidence for a role of the rare p.A152T variant in MAPT in increasing the risk for FTD-spectrum and Alzheimer's diseases. Hum Mol Genet 2012;21:3500–3512. [PubMed: 22556362]

28. Mathis CA, Wang Y, Holt DP, et al. Synthesis and evaluation of 11Clabeled 6-substituted 2-arylbenzothiazoles as amyloid imaging agents. J Med Chem 2003;46:2740–2754. [PubMed: 12801237]

29. Baker SL, Lockhart SN, Price JC, et al. Reference tissue-based kinetic evaluation of 18F-AV-1451 for tau imaging. J Nucl Med 2017;58: 332–338. [PubMed: 27587706]

30. Ashburner J, Ridgway GR. Symmetric diffeomorphic modeling of longitudinal structural MRI. Front Neurosci 2012;6:197. [PubMed: 23386806]

31. Fischl B, Salat DH, Busa E, et al. Whole brain segmentation: automated labeling of neuroanatomical structures in the human brain. Neuron 2002;33:341–355. [PubMed: 11832223]

32. Ashburner J A fast diffeomorphic image registration algorithm. Neuroimage 2007;38:95–113. [PubMed: 17761438]

33. Rousset OG, Ma Y, Evans AC. Correction for partial volume effects in PET: principle and validation. J Nucl Med 1998;39:904–911. [PubMed: 9591599]

34. Baker SL, Maass A, Jagust WJ. Considerations and code for partial volume correcting [18F]-AV-1451 tau PET data. Data Brief 2017;15: 648–657. [PubMed: 29124088]

35. Jack CR, Wiste HJ, Weigand SD, et al. Defining imaging biomarker cut points for brain aging and Alzheimer's disease. Alzheimers Dement 2017;13:205–216. [PubMed: 27697430]

36. Logan J, Fowler JS, Volkow ND, et al. Distribution volume ratios without blood sampling from graphical analysis of PET data. J Cereb Blood Flow Metab 1996;16:834–840. [PubMed: 8784228]

37. Price JC, Klunk WE, Lopresti BJ, et al. Kinetic modeling of amyloid binding in humans using PET imaging and Pittsburgh compound-B. J Cereb Blood Flow Metab 2005;25:1528–1547. [PubMed: 15944649]

38. Maass A, Landau S, Baker SL, et al. Comparison of multiple tau-PET measures as biomarkers in aging and Alzheimer's disease. Neuroimage 2017;157:448–463. [PubMed: 28587897]

39. Jack CR, Wiste HJ, Lesnick TG, et al. Brain β-amyloid load approaches a plateau. Neurology 2013;80:890–896. [PubMed: 23446680]

40. He Z, Guo JL, McBride JD, et al. Amyloid-β plaques enhance Alzheimer's brain tau-seeded pathologies by facilitating neuritic plaque tau aggregation. Nat Med 2017;24:29–38. [PubMed: 29200205]

41. Pooler AM, Polydoro M, Maury EA, et al. Amyloid accelerates tau propagation and toxicity in a model of early Alzheimer's disease. Acta Neuropathol Commun 2015;3:14. [PubMed: 25853174]

42. Leal SL, Lockhart SN, Maass A, et al. Subthreshold amyloid predicts tau deposition in aging. J Neurosci 2018;38:4482–4489. [PubMed: 29686045]

43. Landau SM, Fero A, Baker SL, et al. Measurement of longitudinal β-amyloid change with 18F-florbetapir PET and standardized uptake value ratios. J Nucl Med 2015;56:567–574. [PubMed: 25745095]

44. Goedert M, Masuda-Suzukake M, Falcon B. Like prions: the propagation of aggregated tau and α-synuclein in neurodegeneration. Brain 2017;140:266–278. [PubMed: 27658420]

45. Wang Y, Balaji V, Kaniyappan S, et al. The release and trans-synaptic transmission of tau via exosomes. Mol Neurodegener 2017;12:5. [PubMed: 28086931]

46. Ranganath C, Ritchey M. Two cortical systems for memory-guided behaviour. Nat Rev Neurosci 2012;13:713–726. [PubMed: 22992647]

47. Choi JY, Cho H, Ahn SJ, et al. Off-target ^{18}F-AV-1451 binding in the basal ganglia correlates with age-related iron accumulation. J Nucl Med 2018;59:117–120. [PubMed: 28775201]

48. Lockhart SN, Ayakta N, Winer JR, et al. Elevated 18F-AV-1451 PET tracer uptake detected in incidental imaging findings. Neurology 2017; 88:1095–1097. [PubMed: 28188303]
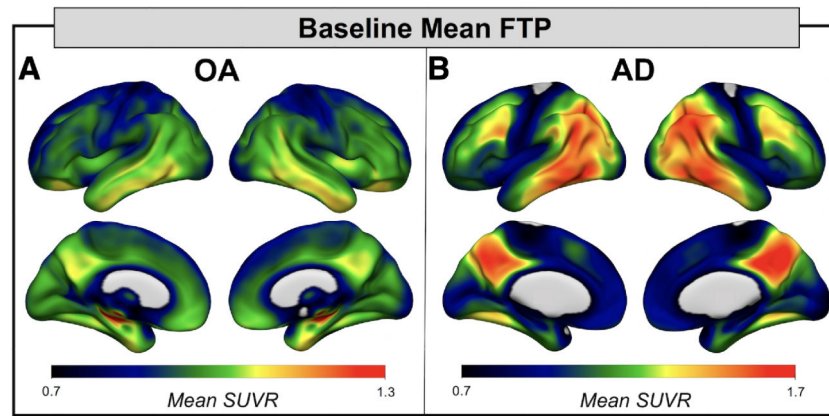
FIGURE 1:

Baseline flortaucipir (FTP) patterns in healthy older adults (OA) and Alzheimer disease (AD) revealed the regions with highest tau burden in each group. (A) Mean group baseline FTP standardized uptake value ratio (SUVR) image for OA (n = 42) reveals that FTP signal is highest in medial temporal lobe, with some signal in the ventral and lateral temporal lobes and in posterior medial regions. (B) Mean group baseline FTP SUVR image for AD (n = 18) reveals high FTP tracer retention in temporal lobe, posterior lateral regions (eg, temporoparietal junction), and posterior medial regions (eg, retrosplenial cortex, posterior cingulate, and precuneus). Note that the upper limit of the color scale was adapted to highlight topology of FTP in each cohort.
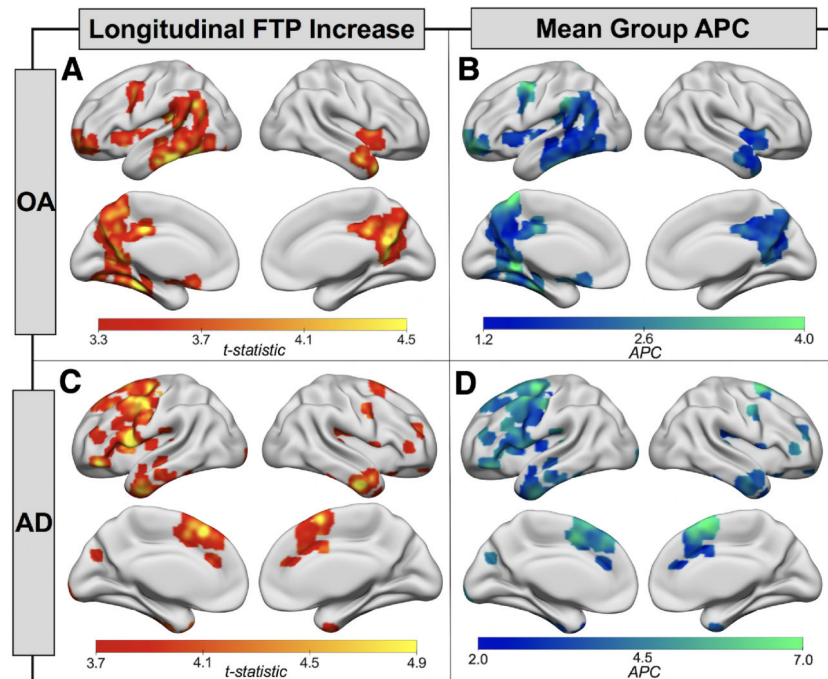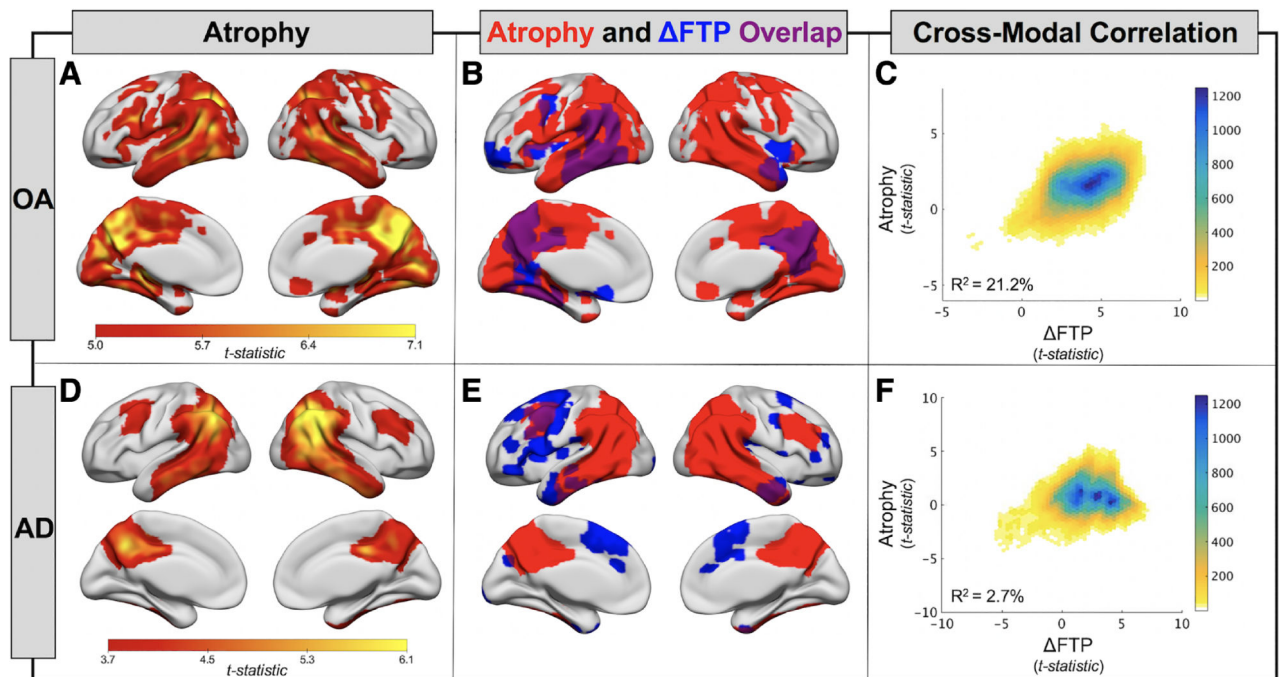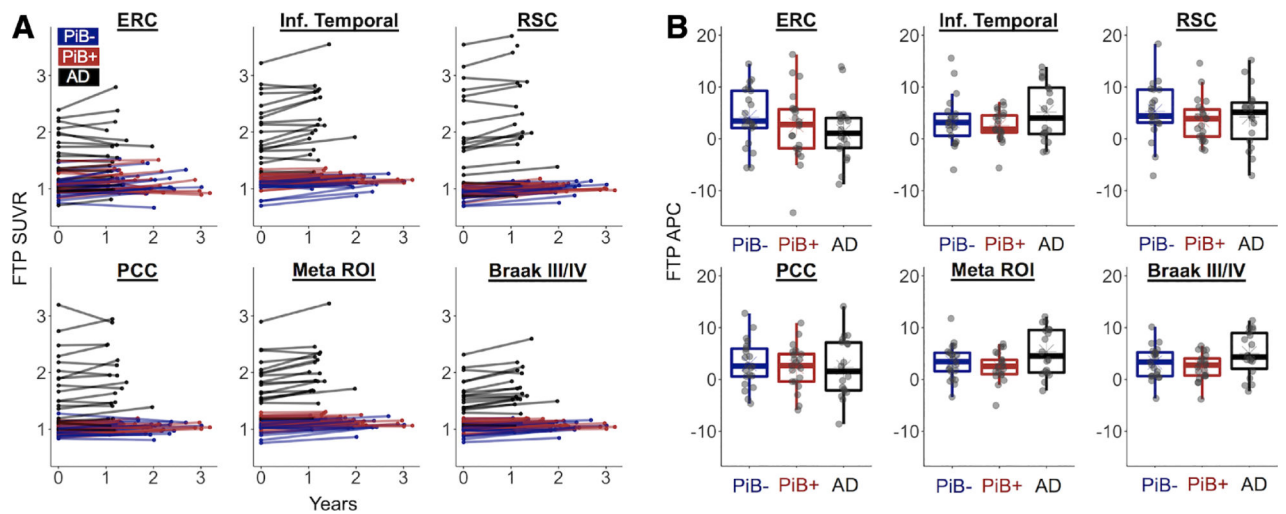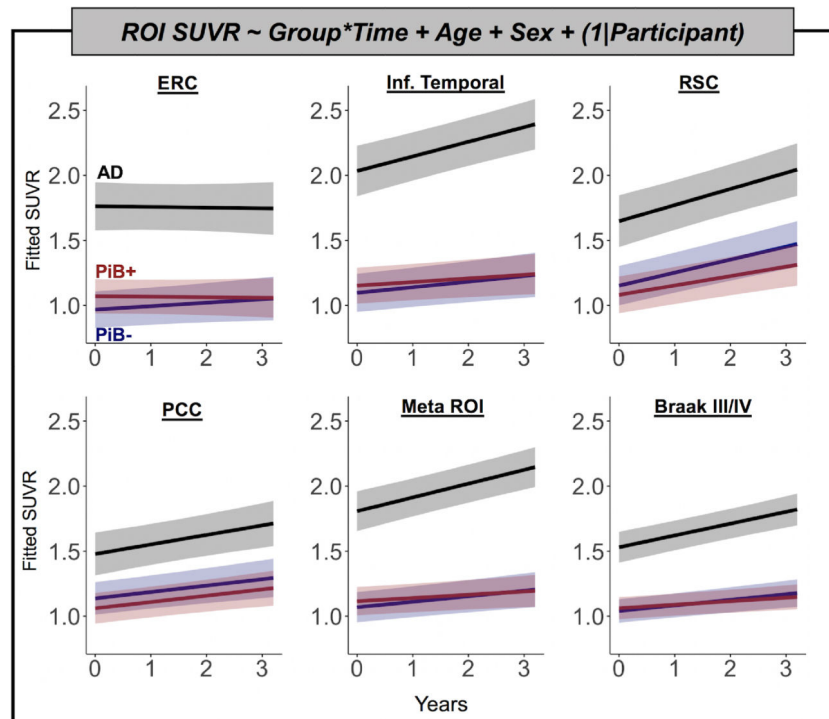
FIGURE 2:

Flortaucipir (FTP) accumulation is spatially distinct in healthy older adults (OA) and Alzheimer disease (AD). (A) Onesample *t* tests show regions where the OA group (n = 42) showed a significant increase in FTP from baseline to follow-up (voxel *p* < 0.001, cluster familywise error *p* < 0.05). (B) Voxelwise mean group annual percentage change (APC) in regions where FTP was significantly increasing (A) in OA. (C) One-sample *t* tests show regions where the AD group (n = 18) showed a significant increase in FTP from baseline to follow-up (voxel *p* < 0.001, uncorrected). (D) Voxelwise mean group APC in regions where FTP was significantly increasing (C) in patients with AD. Note that the upper limits of the color scales in B and D were adapted to highlight variation in mean voxelwise APC in each cohort.

FIGURE 3:

Atrophy and its spatial relationship to flortaucipir (FTP) accumulation in healthy older adults (OA) and Alzheimer disease (AD). (A) One-sample t tests show regions of significant gray matter volume loss in the OA group (n = 42, voxel $p < 0.001$, cluster FWE $p < 0.05$). (B) Overlap (purple) of atrophy pattern from A (red) and pattern of FTP accumulation (blue; see Fig 2A) in OA. (C) Voxelwise cross-modal correlation of t maps from atrophy (A) and FTP accumulation (see Fig 2A) analyses. A linear model was fit to the data to estimate variance explained. Color bar represents the density of points falling within each plotted hexagon. (D) One-sample t tests show regions of significant gray matter volume loss in the AD group (n = 18, voxel $p < 0.001$, uncorrected). (E) Overlap (purple) of atrophy pattern from D (red) and pattern of FTP accumulation (blue; see Fig 2C) in AD. (F) Voxelwise cross-modal correlation of t maps from atrophy (D) and FTP accumulation (see Fig 2C) analyses.

FIGURE 4:

Regional changes in flortaucipir (FTP) have high variance, show no differences based on Pittsburg compound B (PiB) status in healthy older adults, and reveal that patients with Alzheimer disease (AD) have greater FTP accumulation in large regions of interest (ROIs). Regional changes were assessed in 6 ROIs: entorhinal cortex (ERC), inferior (Inf.) temporal cortex, retrosplenial cortex (RSC), posterior cingulate cortex (PCC), a temporal lobe Meta ROI, and Braak III/IV regions. (A) Spaghetti plots show individual trajectories of regional partial volume–corrected standardized uptake value ratio (SUVR) values from baseline to follow-up. (B) Individual annual percentage change (APC) values are plotted by group for each ROI.

FIGURE 5:

Linear mixed effects models show higher flortaucipir (FTP) load and faster accumulation in Alzheimer disease (AD) compared to healthy older adults. Models were fit to predict FTP in 6 regions of interest (ROIs): entorhinal cortex (ERC), inferior (Inf.) temporal cortex, retrosplenial cortex (RSC), posterior cingulate cortex (PCC), a temporal lobe Meta ROI, and Braak III/IV regions. Predicted standardized uptake value ratio (SUVR) values are plotted for each group over time, measured in years. Age and sex were included as fixed covariates of no interest. A random effect of participant intercept was also included in each model. PiB = Pittsburg compound B.

TABLE 1.

Cohort Characteristics

Characteristic	OA, n = 42	AD, n = 19	*p*
Age, yr	77.6 ± 4.6 (68–93)	63.1 ± 10.3 (48–83)	<0.001[a]
Sex, M/F, n	17/25	7/12	0.788
Education, yr	16.4 ± 1.6	17.0 ± 2.1	0.247
PiB +/−, bl, n	21/21	19/0	—
APOEε4 carriers, n	14 (1 NA)	10	0.174
FTP follow-up, yr	1.9 ± 0.6 (1.0–3.2)	1.3 ± 0.3 (1.0–2.2)	<0.001[a]
MMSE[b], bl	28.5 ± 1.3 (25–30)	23.7 ± 4.0 (14–29)	<0.001[a]

Group count data or mean ± standard deviation (range) is shown. OA and AD were compared using 2-sample *t* tests for continuous variables and Fisher exact tests for sex and *APOE* status.

[a]Significant differences at $p < 0.05$ (uncorrected).

[b]Possible range = 0–30.

AD = patients with Alzheimer disease; APOE = apolipoprotein E; bl = baseline; F = female; FTP = flortaucipir; M = male; MMSE = Mini-Mental State Examination; NA = not available; OA = healthy older adults; PiB = Pittsburgh compound B.

Author Manuscript Author Manuscript Author Manuscript Author Manuscript

TABLE 2.

OA versus AD Regional FTP Differences

Region	Baseline FTP SUVR			FTP Annual Percentage Change					
	OA	AD	OA vs AD, p	OA	AD	OA 1-Sample t Test p	AD	AD 1-Sample t Test p	OA vs AD p
ERC	1.07 ± 0.17	1.60 ± 0.50	<0.001[a]	3.40 ± 6.20	1.41 ± 5.97	<0.001[a]		0.329	0.255
IT	1.10 ± 0.13	2.10 ± 0.54	<0.001[a]	3.00 ± 4.00	5.15 ± 5.64	<0.001[a]		0.001[a]	0.095
RSC	0.95 ± 0.11	2.16 ± 0.85	<0.001[a]	4.45 ± 4.90	4.18 ± 5.87	<0.001[a]		0.008[a]	0.854
PCC	1.00 ± 0.10	1.80 ± 0.60	<0.001[a]	2.71 ± 4.32	2.33 ± 5.87	<0.001[a]		0.120	0.779
FOrb	1.02 ± 0.10	1.32 ± 0.55	<0.001[a]	2.56 ± 4.54	5.92 ± 7.70	<0.001[a]		0.005[a]	0.039[a]
IFG	0.99 ± 0.10	1.53 ± 0.46	<0.001[a]	3.53 ± 4.42	7.34 ± 8.14	<0.001[a]		0.001[a]	0.023[a]
Meta ROI	1.07 ± 0.11	1.88 ± 0.41	<0.001[a]	2.89 ± 3.07	5.33 ± 4.62	<0.001[a]		<0.001[a]	0.019[a]
Braak III/IV	1.03 ± 0.10	1.61 ± 0.31	<0.001[a]	2.85 ± 2.88	5.00 ± 4.35	<0.001[a]		<0.001[a]	0.028[a]

Mean ± standard deviation is shown. Groups were compared using 2-sample, 2-sided t tests. One-sample, 2-sided t tests were used to test whether group means significantly differed from zero.

[a] Probability values indicating significant differences at $p < 0.05$ (uncorrected).

AD = patients with Alzheimer disease; ERC = entorhinal cortex; FOrb = orbitofrontal cortex; FTP = flortaucipir; IFG = inferior frontal gyrus; IT = inferior temporal cortex; OA = healthy older adults; PCC = posterior cingulate cortex; ROI = region of interest; RSC = retrosplenial cortex; SUVR = standardized uptake value ratio.

TABLE 3.

LME Model Parameter Estimates

Parameter	Entorhinal Cortex			Temporal Meta ROI			Braak III/IV Regions		
	Beta	CI	p	Beta	CI	p	Beta	CI	p
Fixed effects									
Intercept	−0.17	−1.05 to 0.71	0.706	1.56	0.83 to 2.29	<0.001[a]	1.61	1.05 to 2.18	<0.001[a]
PiB+, vs PiB−	0.10	−0.08 to 0.29	0.274	0.05	−0.11 to 0.20	0.550	0.02	−0.10 to 0.14	0.721
AD, vs PiB−	0.79	0.54 to 1.05	<0.001[a]	0.74	0.53 to 0.95	<0.001[a]	0.49	0.33 to 0.65	<0.001[a]
Time	0.03	−0.00 to 0.06	0.086	0.04	0.02 to 0.06	<0.001[a]	0.04	0.03 to 0.06	<0.001[a]
Age	0.02	0.01 to 0.03	0.004[a]	−0.01	−0.02 to 0.00	0.183	−0.01	−0.01 to 0.00	0.043[a]
M, vs F	−0.17	−0.32 to −0.02	0.029[a]	−0.07	−0.20 to 0.06	0.273	−0.06	−0.16 to 0.04	0.240
PiB+ × Time, vs PiB−	−0.03	−0.07 to 0.01	0.130	−0.02	−0.04 to 0.01	0.153	−0.02	−0.04 to 0.00	0.128
AD × Time, vs PiB−	−0.03	−0.09 to 0.02	0.261	0.06	0.03 to 0.10	<0.001[a]	0.05	0.02 to 0.08	0.001[a]
Random effects									
No. of Participants	60			60			60		
ICC$_{Participant}$	0.910			0.952			0.941		
Observations	120			120			120		
Model fit									
AIC	−0.24			−77.62			−122.66		

All models were estimated in R using lmer4 and the restricted maximum likelihood approach. Probability values were calculated using the Satterthwaite approximation for degrees of freedom.

[a] Probability values indicating significant effects at $p < 0.05$ (uncorrected).

AD = patients with Alzheimer disease; AIC = Akaike information criterion; CI = confidence interval; F = female; ICC = intraclass correlation coefficient; LME = linear mixed effects; M = male; PiB = Pittsburg compound B; ROI = region of interest.